Bandhead energies in ^{125}Cs

Ji Sun (孙吉),[1] Ying-Jun Ma (马英君),[1,*] Tetsuro Komatsubara (小松原哲郎),[2] Kohei Furuno (古野興平),[2]
Yu-Hu Zhang (张玉虎),[3] Wen-Ping Zhou (周文平),[4] Shou-Yu Wang (王守宇),[5] Xue-Yuan Hu (胡雪源),[1] Hao Guo (郭昊),[1]
Jia-Qi Wang (王佳琦),[1] and Yun-Zuo Liu (刘运祚)[1]

[1]*College of Physics, Jilin University, Changchun 130012, China*
[2]*Research Facility Center for Pure and Applied Science, University of Tsukuba, Ibaraki 305-8577, Japan*
[3]*Institute of Modern Physics, Chinese Academy of Sciences, Lanzhou 730000, China*
[4]*Shenyang Institute of Engineering, Shenyang 110136, China*
[5]*Shandong Provincial Key Laboratory of Optical Astronomy and Solar-Terrestrial Environment, School of Space Science and Physics,
Shandong University, Weihai 264209, China*

Excited states in ^{125}Cs have been studied with the fusion-evaporation-reaction ^{116}Cd (^{14}N,5n) at 65-MeV beam energy. The level scheme of ^{125}Cs was extended with the addition of more than 50 new γ transitions and with the identification of two new rotational bands built on the $\pi d_{5/2}$ and $\pi g_{7/2}$ configurations at low spins. The bandhead excitation energies of the previously known $\pi g_{9/2}$ and $\pi h_{11/2}$ bands were revised.

I. INTRODUCTION

Nuclei in the mass region $A \sim 125$ exhibit a richness of nuclear-structure features. Experimental and theoretical studies on nuclei in this region have generated many hot topics, such as the signature inversion [1], competing alignments between the $h_{11/2}$ neutrons and the $h_{11/2}$ protons [2], possible shape coexistence between the prolate and the oblate deformations [3], magnetic dipole band [4], band termination [5], breaking of chiral symmetry [6], and enhancement of octupole correlations [7]. For clear understandings of various nuclear phenomena, adequate and reliable experimental data become particularly crucial. In this connection, bandhead excitation energies associated with different configurations in deformed nuclei are of fundamental importance since they are usually the basis for discussing further topics, such as spin parity and configuration assignments, etc. However, due to the isomeric nature of the bandheads and the high density of nuclear levels at low spins, the measurement of bandhead energies is often a challenge in practice.

The present paper reports on an experimental investigation of the odd-Z even-N nucleus ^{125}Cs. Prior to this paper, it had been studied by many groups. From atomic-beam magnetic resonance [8] and from ^{125}Ba ε decay [9], the ground state of ^{125}Cs is known [10] to have a spin parity of $1/2^+$ and a half-life of 46.7 min. In an earlier in-beam study by Garg *et al.* [11], prolate rotational bands built on the $\pi h_{11/2}[550]1/2^-$, $\pi g_{9/2}^{-1}[404]9/2^+$, and $\pi g_{7/2}[422]3/2^+$ were identified. The $\pi h_{11/2}$ bandhead was recognized to be an isomer and was located at an excitation energy of 266 keV. Meanwhile, the $\pi g_{9/2}$ bandhead was connected to the $11/2^-$ bandhead state through an intense 275-keV $E1$ ($9/2^+ \to 11/2^-$) transition. These experimental results were adopted or corroborated by later studies [10,12,13]. In the recent study by Singh *et al.* [14], the earlier reported [11,12] 275-keV transition was reassigned as an in-band $11/2^+ \to 9/2^+ M1$

transition according to systematics. However, because of the lack of direct experimental evidence, this reassignment was not adopted in the subsequent compilation for $A = 125$ nuclei [10]. In this paper the above-mentioned $11/2^-$ and $9/2^+$ bandhead energies in ^{125}Cs have been newly established on the basis of direct and firm experimental evidence.

The $\pi g_{7/2}[422]3/2^+$ and $\pi d_{5/2}[420]1/2^+$ are two other Nilsson orbitals in vicinity of the $Z = 55$ proton Fermi surface at prolate deformations. Rotational bands built on the two configurations have been systematically established in heavier odd-A Cs isotopes with $A \geq 127$ [15–20], whereas in lighter odd-A Cs isotopes only one $\Delta I = 2$ sequence built on the $g_{7/2}$ configuration has been reported so far [11–14,21–28]. The two orbitals lie very close to each other and form the pseudospin doublet state $\widetilde{[321]}$. Both experimental and theoretical studies indicate that they are strongly mixed, which presents a challenge to the experimental discrimination between them. Indeed, in the recent spectroscopic study of ^{129}Cs, Sihotra *et al.* [18] proposed an alternative prescription (see Sec. IV) for the configuration assignments of the observed low-lying positive-parity $\pi g_{7/2}$ and $\pi d_{5/2}$ bands. Systematics extending the observation of similar structures down to ^{125}Cs will be informative for distinguishing between the two different prescriptions.

II. EXPERIMENTAL METHODS AND DATA ANALYSIS

Excited states in ^{125}Cs were produced via the ^{116}Cd (^{14}N,5n) fusion-evaporation reaction in the course of an experiment whose main objective was the study of ^{126}Cs [29]. The experiment was carried out at the Niels Bohr Institute (NBI), Denmark. The FN tandem accelerator system provided a 65-MeV ^{14}N beam which bombarded a target consisting of a 0.82-mg cm^{-2} ^{116}Cd foil backed with 1-mg cm^{-2}Au. γ rays emitted from the reaction were measured using the NORDBALL detector array [30], which consisted, for this experiment, of 19 anti-Compton HPGe spectrometers (ACSs) and a planar low-energy photon HPGe spectrometer (LEPS). A coincidence resolving time of $2\tau = 100$ ns was used to collect the γ-γ coincidence data. The detectors were mounted on four

different rings at 37°, 79°, 101°, and 143° with respect to the beam direction. Their energy and efficiency calibrations were made using standard ^{152}Eu and ^{133}Ba sources.

In the off-line analysis, the γ-γ coincidence data recorded from the 19 ACS detectors were recalibrated to 0.5 keV/channel and then sorted, event by event, into a two-dimensional 4096×4096 symmetrized E_γ-E_γ matrix. Its full projection contains about $8 \times 10^8 \gamma$-γ coincidence events. To aid the analysis of coincidence relationships associated with low-energy γ rays, an asymmetric two-dimensional 2048×2048 matrix was constructed with the LEPS data on one axis (0.25 keV/channel) and the 19 ACSs data on the other axis (0.5 keV/channel). γ-rays' relative intensities were, where possible, established from the full projection of the 4096×4096 symmetrized E_γ-E_γ matrix. For weak or unsolvable lines, they were established from coincidence spectra under appropriate gating conditions. In cases where a level is depopulated by several transitions in order to reflect the branching ratios as precisely as possible, the relative intensities of these transitions were preferably determined by gating on transition(s) populating the level. The uncertainties of relative intensities were calculated from the statistical and systematical uncertainties. As to systematical uncertainties, we principally considered the effects of uncertainties of the efficiency calibration. The systematical uncertainties are estimated as 4% for transitions above 180 keV. For transitions below 180 keV the systematical uncertainties were estimated as 6%–20% because the efficiency curve as a function of transition energy varies rapidly in the low-energy region, particularly in the region below 100 keV.

In order to obtain information on the γ-ray multipolarities, two angular distribution matrices were constructed using the same method as described in papers, e.g., Refs. [31,32], which also report in-beam experiments performed with the NORDBALL detector array at the NBI. The first matrix was created with events detected in detectors at 37° (or the equivalent 143°) on one axis (denoted as the x axis) and those in all detectors on the other axis (denoted as the y axis). Similarly the second matrix contained events detected in detectors at 79° (or the equivalent 101°) on the x axis and those in all detectors on the y axis. Then, γ-ray angular distribution ratios from oriented nuclei (ADO) were evaluated from these asymmetric matrices. The ADO ratio is defined as $R_{\text{ADO}} = I_\gamma(37°)/I_\gamma(79°)$. Here $I_\gamma(37°)$ corresponds to the γ-ray coincidence intensity observed by detectors at either 37° or 143° from the x axis of one of the two asymmetric matrices, and $I_\gamma(79°)$ corresponds to the γ-ray coincidence intensity observed by detectors at either 79° or 101° from the x axis of the other asymmetric matrix. In obtaining $I_\gamma(37°)$ and $I_\gamma(79°)$, identical gates were set in the corresponding matrix on the axis with events detected in all detectors (y axis). Efficiency normalizations for $I_\gamma(37°)$ and $I_\gamma(79°)$, respectively, were performed utilizing the efficiency curves of detectors at corresponding angles. The uncertainty of the ADO ratio of a γ ray was computed according to the standard-deviation criterion. For contaminated or weak γ rays, the relative uncertainties of their ADO ratios were further enlarged by about 10%. As demonstrated in Refs. [3,31,32], and the γ-ray intensities extracted from the two asymmetric

matrices follow the empirical angular distribution law $W(\theta) \approx I_\gamma[1 + A_2 P_2(\cos \theta)]$ as a function of the detector angle θ relative to the beam direction, where $P_2(\cos \theta)$ is the Legendre polynomials. Thus the ADO ratio for transitions having positive (negative) coefficient A_2 values is expected to be greater (less) than 1.0. In practice, by examining the strong γ rays with known multipolarities contained in our data, the ADO ratios for stretched quadrupole and dipole transitions are found to be ≈ 1.4 and ≈ 0.7, respectively. These empirical laws can thus be used to assist us in the multipolarity assignments for newly observed γ rays of interest. It is noted that values of $R_{\text{ADO}} \approx 1.4$ may alternatively correspond to $\Delta I = 0$ unstretched transitions or certain strongly mixed $\Delta I = 1$ transitions. Parallel decay pathways and crossover connections in the level scheme may provide further arguments for distinguishing between these possibilities. It is also noted that for γ transitions following the decay of an isomer with relatively long lifetime, the extraction of their ADO ratios is no longer so meaningful since the long lifetime will cause a dealignment of the originally oriented nucleus.

After careful and comprehensive analysis, it was realized that γ rays from the following nuclei can be identified from our coincidence data: ^{124,125,126,127}Cs ($Z = 55$), ^{124,125,126,127}Xe ($Z = 54$), ^{122,123,124}I ($Z = 53$), ^{118,120,122}Te ($Z = 52$), ^{119,120,121}Sb ($Z = 51$), ^{116,118,120}Sn ($Z = 50$), ^{117}In ($Z = 49$), ^{114,116}Cd ($Z = 48$), and ^{197}Au ($Z = 79$). The information of some other nuclei, e.g., ^{119,121}Te and the daughter nuclei of those unstable products, must also be contained in our data. However, due to very low yields, γ transitions from them smeared out into the background and thus could not be identified clearly. On the whole, the observed relative yield of residual nucleus shows decreasing trend with increasing number of protons evaporated from the compound nucleus ^{130}Cs. Furthermore, there is a trend of enhancement in the observed yield if one or two α particles may evaporate collectively from the compound nucleus ^{130}Cs. Among the above-listed nuclei, the nucleus ^{126}Cs was produced with the largest yield, and ^{125}Cs and ^{123}I are two other nuclei whose excited states were strongly populated in the used reaction. Major results for ^{126}Cs and ^{123}I have been reported in our previous papers [6,33,3,34]. ^{126}Xe and ^{127}Cs are the next two nuclei with relatively large yields. About 70% of the known γ transitions in them [35,15] can be identified with our data. For the other nuclei listed above, only very a few intense transitions in them can be identified due to very low relative yields. We finally note that: (1) The nucleus ^{117}In observed in our data was produced from one-proton transfer reaction; (2) the observations of γ rays from ^{114,116}Cd and ^{197}Au resulted from the Coulomb excitations of the Cd target and Au backing; (3) the appearance of γ rays from ^{114}Cd should be relevant to the purity of the Cd target; and (4) no evidence could be found for the possible occurrence of nuclear reaction between the ^{14}N beams and the ^{197}Au backing.

The analysis of coincidence relations was performed with twofold coincidence spectra, which would sometimes inevitably introduce contamination lines into the gating spectra. There are many techniques for discriminating contamination lines as exemplified below. For the case where the peak of

a gating γ ray is overlapped by the tail or shoulder of the peak of a contaminating γ ray, the coincidences introduced by the latter can be easily excluded in most cases by watching the variations of coincidence intensities of various γ peaks with the shift of the centroid of the gating window. For the case where the gating and contaminating γ rays have very close energies (with difference less than about 0.5 keV), the clues for excluding contamination lines can generally be found from coincidence spectra gating on other γ rays particularly those γ rays parallel to the γ ray of interest. Coincidence intensity can generally provide very important information for the analysis of coincidence relations. For instance, if a newly observed coincidence relation is even obviously stronger than the strongest coincidence known in a certain nucleus in the same data, it is unlikely that the newly observed coincidence is from that nucleus. In a group consisting of some mutually coincident and some mutually noncoincident γ rays, energy-sum relationships among these γ rays can provide a further check for the suggested coincidence structure. Above all, the assignment of new γ rays and the construction of new coincidence structures in ^{125}Cs relied not only on a certain single argument, and actually, we have performed a very comprehensive analysis of each line in the coincidence spectra of the γ rays of interest.

III. EXPERIMENTAL RESULTS

The level scheme derived for ^{125}Cs is presented in Fig. 1 wherein the band structures have been labeled 1–10 to facilitate the discussion. The placement of γ transitions in the level scheme is based on their intensities, energy sums, and coincidence relationships. Spin-parity assignments to the observed levels are based on the probable multipolarities inferred from the measured ADO ratios of the related transitions and on the previous knowledge about ^{125}Cs [8–14]. Figure 2 displays some examples of coincidence spectra. Table I provides a summary of all ^{125}Cs transitions observed in the measurement. In comparison to the previous studies, new major features of the present level scheme of ^{125}Cs are given below.

Band 9 is the most intensely populated band in ^{125}Cs and is known [10] to be built on the $h_{11/2}[550]1/2^-$ configuration. Similar to the behavior of high-j low-Ω bands in many odd-A nuclei, the level energy $E(I)$ of this band as a function of spin I shows a parabolalike curve with the $I = j = 11/2$ state being the lowest member of the band. States with $I < j$ lie far away from the yrast line and are thereby difficult to be observed via fusion-evaporation reactions. Previous studies [11–14] had ascertained the isomeric nature of the $11/2^-$ bandhead. Based on the assumption of an unobserved 13-keV $11/2^- \rightarrow 7/2^+$ $M2$ transition and on the observation of a weak 189-keV transition linking the $11/2^-$ bandhead state to the state with known excitation energy (77 keV), the excitation energy of the $11/2^-$ bandhead state was determined to be 266 keV by Garg *et al.* [11]. In the present investigation, the previously reported [11] 189-keV transition linking the $11/2^-$ isomer to the state at 77 keV cannot be confirmed. Instead, we have been able to find a large number of transitions through which band 9 can be connected to states with known excitation energies, such as the 1023.2-, 1206.1-, 1017.8-, and

1246.2-keV transitions (cf. Fig. 1). The observed coincidences as exemplified in Figs. 2(a), 2(f)–2(h), support strongly the linking patterns of band 9 with other bands relevant. In fact, the decay of the high-lying band 5 to band 9 and to band 3 had also been noticed previously by Singh *et al.* [14], although the detailed decay pathways were not established in their work due to the diffluence of the intensity flow. Besides, the coincidence between intense transitions in the high-lying band 6 and the 168.4-keV transitions near the bottom of band 3 can be inferred from the example spectrum in Ref. [14]. Based on these self-consistent observations, the bandhead energy of band 9 is ascertained to be 294 keV rather than the previously reported [10–14] 266 keV. In addition, an unobserved 41-keV $M2$ transition is expected to be present between the $11/2^-$ state of band 9 and the $7/2^+$ state of band 3. The calculation of the newly suggested bandhead energy has to be performed along a chain comprising at least seven transitions [e.g., $77.4(3) + 176.2(2) + 430.4(2) + 1023.2(8) + 648.3(8) - 1695.6(8) - 365.8(2) = 294.1 \text{keV}$], hence the maximum uncertainty of the bandhead energy of 294 keV is estimated to be 3.3 keV.

Band 4 was previously connected to the $11/2^-$ state in band 9 via an intense 275-keV transition as well as a weak 585-keV transition [11,12]. Apparently, such a connecting mode should be regarded as tentative level scheme since no appropriate transitions below the $11/2^-$ state can offer a further check for their proposed coincidence relationships. In fact, a strong coincidence between band 4 and transitions near the ground state can be inferred from Fig. 2(a). After careful analysis of the coincidence data, we have established the decay paths from band 4 to lower-lying states; see Fig. 1. Although the 309.6-, 377.8-, and 478.1-keV linking transitions are not so weak, they are seriously contaminated, presenting an obstacle to the positioning of band 4. As seen in Fig. 1, the 309.6- and 377.8-keV transitions are both doublet lines. The 478.1-keV linking transition is seriously contaminated by a 478.1-keV transition in the yrast band from the accompanying nucleus ^{126}Cs [6] and by the 475.6- and 480.3-keV transitions in band 8 of ^{125}Cs. To show the complex coincidence relationships, we present four examples of coincidence spectra in Figs. 2(a)– 2(d). Based on these observations, the bandhead of band 4 is located at an excitation energy of 563 keV. In addition, the previously reported 275- and 585-keV transitions have been reassigned as the in-band $11/2^+ \rightarrow 9/2^+$ and $13/2^+ \rightarrow 9/2^+$ transitions of the $\pi g_{9/2}^{-1}[404]9/2^+$ band. The above revisions fit well to the systematics of the $\pi g_{9/2}^{-1}[404]9/2^+$ bands in odd-A Cs isotopes as discussed in Ref. [14].

It is worthwhile to explain why the doublet lines with $E_\gamma \approx 310$ and 378 keV are from ^{125}Cs. In the spectrum shown in Fig. 2(a), it is seen that the coincidence intensity of the line at 310 keV is obviously greater than that of the line at 275 keV contrary to the usual expectation if the line at 310 keV is assumed to be a single line. The 310.0-keV transition in band 4 lies farther away from the 168.4-keV gating transition than the 275.1 keV transition in band 4, and thus a weaker coincidence with the 168.4-keV transition is expected for the 310.0-keV transition. Therefore, the relatively stronger peak at 310 keV strongly implies that two γ rays with energy of 310 keV are in coincidence with the 168-keV transition. The spectrum

TABLE I. Measured properties of γ rays in ^{125}Cs. Transitions or levels observed for the first time are marked with asterisks (*).

E_γ (keV)[a]	E_i (keV)[b]	Band	Spin-parity assignment	I_γ[c]	R_{ADO}[d]
41*[e]	294.1	9 → 3	$11/2^- \rightarrow 7/2^+$		
71.1*	2426.8	6	$19/2^+ \rightarrow 17/2^+$	29(20)	
77.4	77.4	3 → 2	$3/2^+ \rightarrow 1/2^+$	68(30)[f]	0.76(25)
78.2	2426.8	6	$19/2^+ \rightarrow 17/2^+$	43(15)	0.82(23)
85.1	85.1	2	$5/2^+ \rightarrow 1/2^+$	71(18)[f]	1.38(27)
100.4	185.1	1 → 2	$5/2^+ \rightarrow 5/2^+$	<4	
107.7	185.1	1 → 3	$5/2^+ \rightarrow 3/2^+$	<5	
122.1	2548.9	6	$21/2^+ \rightarrow 19/2^+$	185(12)	0.81(6)
168.4	253.6	3 → 2	$7/2^+ \rightarrow 5/2^+$	137(9)[f]	0.86(7)
176.2	253.6	3	$7/2^+ \rightarrow 3/2^+$	111(7)[f]	1.41(11)
180.6	2729.5	6	$23/2^+ \rightarrow 21/2^+$	201(11)	0.78(5)
190.2*	2837.4*	7	$21/2^+ \rightarrow 19/2^+$	3(2)	
201.0*	3038.4*	7	$23/2^+ \rightarrow 21/2^+$	<2	
212.6*	466.1*	2 → 3	$9/2^+ \rightarrow 7/2^+$	9(4)	0.80(10)
213.5*	2946.8	3 → 2	$23/2^+ \rightarrow 21/2^+$	7(4)	0.81(24)
217.9*	684.0	3 → 2	$11/2^+ \rightarrow 9/2^+$	< 2	
232.1*	3270.7	7	$25/2^+ \rightarrow 23/2^+$	9(5)	0.85(19)
235.6	4626.4	9	$35/2^- \rightarrow 33/2^-$	<2	
246.5	2976.2	6	$25/2^+ \rightarrow 23/2^+$	166(10)	0.77(5)
275.1	838.3	4	$11/2^+ \rightarrow 9/2^+$	86(8)	0.81(8)
287.6*	3558.7*	7	$27/2^+ \rightarrow 25/2^+$	13(5)	0.76(19)
290.5*	3529.2*	3 → 2	$27/2^+ \rightarrow 25/2^+$	11(4)	0.79(31)
292.3*	3238.7*	2 → 3	$25/2^+ \rightarrow 23/2^+$	23(6)	0.73(13)
306.0	5553.4	9	$39/2^- \rightarrow 37/2^-$	<3	
309.6*	563.2	4 → 3	$9/2^+ \rightarrow 7/2^+$	45(15)	0.81(23)
310.0	1148.4	4	$13/2^+ \rightarrow 11/2^+$	68(20)	0.82(22)
311.8	3288.2	6	$27/2^+ \rightarrow 25/2^+$	152(10)	0.77(5)
312.2*	3871.1	7	$29/2^+ \rightarrow 27/2^+$	15(9)	
316.4*	3238.7*	2 → 3	$25/2^+ \rightarrow 23/2^+$	<3	
330.8	6556.1	9	$43/2^- \rightarrow 41/2^-$	<2	
346.2	1494.6	4	$15/2^+ \rightarrow 13/2^+$	61(6)	0.83(9)
355.8*	609.4*	1 → 3	$9/2^+ \rightarrow 7/2^+$	15(5)	0.60(12)
359.9	3648.1	6	$29/2^+ \rightarrow 27/2^+$	113(8)	0.65(5)
362.6*	1046.8*	2 → 3	$13/2^+ \rightarrow 11/2^+$	5(3)	0.81(21)
365.8	659.9	9	$15/2^- \rightarrow 11/2^-$	≡1000	1.36(9)
371.7	4243.0	7	$31/2^+ \rightarrow 29/2^+$	19(6)	0.78(18)
377.8*	563.2	4 → 1	$9/2^+ \rightarrow 5/2^+$	35(13)	1.29(28)
378.7	1873.2	4	$17/2^+ \rightarrow 15/2^+$	59(20)	0.79(23)
381.0*	466.1	2	$9/2^+ \rightarrow 5/2^+$	84(7)	1.34(10)
389.6*	3918.8	2 → 3	$29/2^+ \rightarrow 27/2^+$	<3	
392.5	4635.3	7	$33/2^+ \rightarrow 31/2^+$	9(6)	
393.4	4041.5	6	$31/2^+ \rightarrow 29/2^+$	71(7)	0.78(6)
410.7*	2837.4*	7 → 6	$21/2^+ \rightarrow 19/2^+$	<3	
411.8	2285.2	4	$19/2^+ \rightarrow 17/2^+$	29(6)	0.63(15)
424.1	5059.4	7	$35/2^+ \rightarrow 33/2^+$	<4	
424.3*	609.4*	1	$9/2^+ \rightarrow 5/2^+$	39(7)	1.38(18)
430.4	684.0	3	$11/2^+ \rightarrow 7/2^+$	195(12)	1.42(10)
439.7	2724.8	4	$21/2^+ \rightarrow 19/2^+$	15(5)	0.80(20)
441.6	4483.2	6	$33/2^+ \rightarrow 31/2^+$	34(6)	0.63(9)
454.6*	1302.5*	8 → 9	$15/2^- \rightarrow 13/2^-$	35(6)	0.62(9)
460.1*	1307.8	9	$17/2^- \rightarrow 13/2^-$	22(6)	1.35(13)
470.8	3195.4	4	$23/2^+ \rightarrow 21/2^+$	8(4)	0.77(30)
474.8	4958.0	6	$35/2^+ \rightarrow 33/2^+$	19(6)	0.64(10)
475.6	1782.8	8 → 9	$19/2^- \rightarrow 17/2^-$	79(10)	0.70(9)
478.1*	563.2	4 → 2	$9/2^+ \rightarrow 5/2^+$	8(4)	1.37(19)
480.3*	1782.8	8	$19/2^- \rightarrow 15/2^-$	21(5)	1.32(12)
489.8*	3038.4*	7 → 6	$23/2^+ \rightarrow 21/2^+$	9(4)	0.76(18)

TABLE I. (*Continued.*)

E_γ (keV)[a]	E_i (keV)[b]	Band	Spin-parity assignment	I_γ[c]	R_{ADO}[d]
490.0	3685.1	4	$25/2^+ \to 23/2^+$		
501.0*	3049.1	$5 \to 6$	$23/2^+ \to 21/2^+$	<5	
504.1	5462.0	6	$37/2^+ \to 35/2^+$	10(5)	0.67(30)
505.8*	3238.7*	2	$25/2^+ \to 21/2^+$	<5	
525.9	2454.8	$8 \to 9$	$23/2^- \to 21/2^-$	51(6)	0.77(20)
535.4*	3049.1	5	$23/2^+ \to 19/2^+$	15(5)	1.42(13)
541.6	3270.7	$7 \to 6$	$25/2^+ \to 23/2^+$	21(6)	0.68(13)
553.4*	847.7*	9	$13/2^- \to 11/2^-$	27(7)	0.64(8)
558.9	3288.2	6	$27/2^+ \to 23/2^+$	12(5)	1.54(21)
572.8	1232.7	9	$19/2^- \to 15/2^-$	663(30)	1.46(10)
577.3	5059.4	$7 \to 6$	$35/2^+ \to 33/2^+$	5(3)	
580.8*	1046.8*	2	$13/2^+ \to 9/2^+$	74(7)	1.36(10)
582.6*	3529.2*	3	$27/2^+ \to 23/2^+$	13(6)	1.41(16)
582.9*	3558.7*	$7 \to 6$	$27/2^+ \to 25/2^+$	30(6)	0.70(15)
583.0	3871.1	$7 \to 6$	$29/2^+ \to 27/2^+$	21(9)	0.66(16)
585.2	1148.4	4	$13/2^+ \to 9/2^+$	7(4)	
593.8	4635.3	$7 \to 6$	$33/2^+ \to 31/2^+$	8(5)	
594.6	4243.0	$7 \to 6$	$31/2^+ \to 29/2^+$	20(5)	0.74(13)
607.6	3209.3	10	$27/2^- \to 23/2^-$	12(5)	1.47(22)
610.7	1294.7	3	$15/2^+ \to 11/2^+$	181(13)	1.38(10)
611.2	3660.1	5	$27/2^+ \to 23/2^+$	20(6)	1.37(15)
616.9*	1226.3*	1	$13/2^+ \to 9/2^+$	31(6)	1.34(19)
620.7	5247.0	9	$37/2^- \to 35/2^-$	11(4)	0.69(15)
621.0	1929.0	9	$21/2^- \to 17/2^-$	97(8)	1.42(9)
632.2*	3238.7*	2	$25/2^+ \to 21/2^+$	26(7)	1.45(11)
634.9	4390.6	9	$33/2^- \to 31/2^-$	13(4)	0.50(12)
641.4*	2348.6	$6 \to 3$	$17/2^+ \to 13/2^+$	<6	
647.9	1307.8	9	$17/2^- \to 15/2^-$	284(15)	0.55(6)
648.3*	2355.8*	$6 \to 3$	$17/2^+ \to 13/2^+$	6(3)	
656.3	1494.6	4	$15/2^+ \to 11/2^+$	30(6)	1.29(14)
669.8	6223.1	9	$41/2^- \to 39/2^-$	<6	
671.5	2454.8	8	$23/2^- \to 19/2^-$	113(9)	1.36(12)
672.0	3648.1	6	$29/2^+ \to 25/2^+$	22(7)	1.34(14)
680.1*	3918.8*	2	$29/2^+ \to 25/2^+$	11(4)	1.32(16)
686.6[g]	3997.4		$(31/2^-) \to 27/2^-$	<6	
696.3	1929.0	9	$21/2^- \to 19/2^-$	230(12)	0.59(6)
721.4	3584.9	9	$29/2^- \to 27/2^-$	19(6)	0.80(15)
722.1	3270.7	$7 \to 6$	$25/2^+ \to 21/2^+$	<7	
724.8	1873.2	4	$17/2^+ \to 13/2^+$	26(7)	1.32(15)
728.4	2721.5	9	$25/2^- \to 23/2^-$	58(7)	0.52(13)
737.6*	3660.1	$5 \to 3$	$27/2^+ \to 23/2^+$	<7	
738.3*	1785.1*	2	$17/2^+ \to 13/2^+$	65(7)	1.42(11)
744.1	4404.2	5	$31/2^+ \to 27/2^+$	24(7)	1.34(12)
753.2	4041.5	6	$31/2^+ \to 27/2^+$	24(7)	1.36(15)
760.4	1993.1	9	$23/2- \to 19/2-$	524(24)	1.33(9)
762.4	2057.1	3	$19/2^+ \to 15/2^+$	137(10)	1.33(11)
765.5	2548.9	$6 \to 8$	$21/2^+ \to 19/2-$	72(9)	0.82(12)
772.5*	1998.8*	1	$17/2^+ \to 13/2^+$	18(6)	1.41(20)
790.7	2285.2	4	$19/2^+ \to 15/2^+$	22(7)	1.25(19)
792.6	2721.5	9	$25/2^- \to 21/2^-$	81(7)	1.46(9)
798.3	4007.8	10	$31/2^- \to 27/2^-$	<7	
805.9	4390.6	9	$33/2^- \to 29/2^-$	15(5)	1.33(12)
820.8	3275.6	8	$27/2^- \to 23/2^-$	57(7)	1.48(13)
821.4*	2606.5*	2	$21/2^+ \to 17/2^+$	48(7)	1.41(10)
829.5*	3558.7	$7 \to 6$	$27/2^+ \to 23/2^+$	<8	
832.6	5236.8	5	$35/2^+ \to 31/2^+$	17(7)	1.38(15)
835.2	4483.2	6	$33/2^+ \to 29/2^+$	21(7)	1.30(14)

TABLE I. (*Continued.*)

E_γ (keV)[a]	E_i (keV)[b]	Band	Spin-parity assignment	I_γ[c]	R_{ADO}[d]
842.8	(5247.0)*			17(7)	1.37(19)
851.3	2724.8	4	$21/2^+ \rightarrow 17/2^+$	20(7)	1.38(16)
854.5*	2853.3*	1	$21/2^+ \rightarrow 17/2^+$	8(4)	1.45(23)
856.2	5247.0	9	$37/2^- \rightarrow 33/2^-$	8(4)	
863.5	3584.9	9	$29/2^- \rightarrow 25/2^-$	21(6)	1.51(12)
865.2	2922.3	3	$23/2^+ \rightarrow 19/2^+$	65(8)	1.37(12)
870.2	2863.3	9	$27/2^- \rightarrow 23/2^-$	213(33)	1.37(23)
870.9	4626.4	9	$35/2^- \rightarrow 31/2^-$	68(15)	
871.5	6108.3	5	$39/2^+ \rightarrow 35/2^+$	9(6)	1.32(21)
883.5*	4159.1*	8	$31/2^- \rightarrow 27/2^-$	32(6)	1.41(15)
889.7	2946.8	3	$23/2^+ \rightarrow 19/2^+$	40(6)	1.35(13)
892.1	3755.5	9	$31/2^- \rightarrow 27/2^-$	116(8)	1.38(11)
895.4	3871.1	$7 \rightarrow 6$	$29/2^+ \rightarrow 25/2^+$	11(4)	1.35(20)
910.0	3195.4	4	$23/2^+ \rightarrow 19/2^+$	<9	
915.7	4958.0	6	$35/2^+ \rightarrow 31/2^+$	14(5)	1.43(30)
927.0	5553.4	9	$39/2^- \rightarrow 35/2^-$	31(6)	1.33(14)
945.2	4953.6	10	$35/2^- \rightarrow 31/2^-$	<9	
948.2*	2732.9*	2	$21/2^+ \rightarrow 17/2^+$	11(4)	1.36(18)
949.3	7057.6	5	$(43/2^+) \rightarrow 39/2^+$	<9	
955.0	4243.0	$7 \rightarrow 6$	$31/2^+ \rightarrow 27/2^+$	9(5)	
960.0	3685.1	4	$25/2^+ \rightarrow 21/2^+$		
975.7	6223.1	9	$41/2^- \rightarrow 37/2^-$	<5	
978.7	5462.0	6	$37/2^+ \rightarrow 33/2^+$	10(4)	1.28(30)
987.2	4685.3	$7 \rightarrow 6$	$33/2^+ \rightarrow 29/2^+$	<9	
992.0*	3049.1	$5 \rightarrow 3$	$23/2^+ \rightarrow 19/2^+$	<7	
1001.7	6556.1	9	$43/2^- \rightarrow 39/2^-$	13(4)	1.26(31)
1009.0*	1302.5*	$8 \rightarrow 9$	$15/2^- \rightarrow 11/2^-$	<10	
1011.4	5969.4	6	$(39/2^+) \rightarrow 35/2^+$	<10	
1017.8*	2946.8	$3 \rightarrow 9$	$23/2^+ \rightarrow 21/2^-$	23(7)	0.64(9)
1023.2*	1707.2*	$6 \rightarrow 3$	$13/2^+ \rightarrow 11/2^+$	12(4)	0.58(13)
1040.0	6502.0	6	$(41/2^+) \rightarrow 37/2^+$	<10	
1061.1*	2355.8*	$6 \rightarrow 3$	$17/2^+ \rightarrow 15/2^+$	<10	
1109.0*	3038.4*	$7 \rightarrow 9$	$23/2^+ \rightarrow 21/2^-$	14(5)	0.59(21)
1115.9*	2348.6	$6 \rightarrow 9$	$17/2^+ \rightarrow 19/2^-$	16(5)	0.80(15)
1119.0	2426.8	$6 \rightarrow 9$	$19/2^+ \rightarrow 17/2^-$	130(9)	0.71(6)
1123.3	1782.8	$8 \rightarrow 9$	$19/2^- \rightarrow 15/2^-$	37(7)	1.42(18)
1144.8	4007.8	$10 \rightarrow 9$	$31/2^- \rightarrow 27/2^-$	21(7)	1.25(11)
1198.3	4953.6	$10 \rightarrow 9$	$35/2^- \rightarrow 31/2^-$	<10	
1206.1*	2513.7*	$5 \rightarrow 9$	$19/2^+ \rightarrow 17/2^-$	17(5)	0.68(9)
1216.3	3209.3	$10 \rightarrow 9$	$27/2^- \rightarrow 23/2^-$	31(6)	1.47(10)
1221.8	2554.8	$8 \rightarrow 9$	$23/2^- \rightarrow 19/2^-$	<10	
1246.2*	3238.7	$2 \rightarrow 9$	$25/2^+ \rightarrow 23/2^-$	<10	
1316.3*	2548.9	$6 \rightarrow 9$	$21/2^+ \rightarrow 19/2^-$	<10	
1317.7[g]	3310.8		$27/2^- \rightarrow 23/2^-$	16(5)	1.40(18)
1339.3*	2647.1*	$7 \rightarrow 9$	$19/2^+ \rightarrow 17/2^-$	<5	
1368.7	2601.4	$10 \rightarrow 9$	$23/2^- \rightarrow 19/2^-$	25(7)	1.27(11)
1500.8*[g]	2732.9*	$2 \rightarrow 9$	$21/2^+ \rightarrow 19/2^-$	11(4)	0.74(10)
1688.2	2348.6	$6 \rightarrow 9$	$17/2^+ \rightarrow 15/2^-$	60(6)	0.79(8)
1695.9*	2355.8	$6 \rightarrow 9$	$17/2^+ \rightarrow 15/2^-$	13	0.74(10)

[a]Uncertainties in the energies of the observed γ ray is between 0.2 and 0.8 keV depending on their intensity.

[b]Absolute excitation energy of the depopulated state.

[c]Relative intensities normalized to the 365.8 keV transition with $I_\gamma = 1000$.

[d]ADO ratios extracted using the procedure as described in Sec. II.

[e]Unobserved; see the text for the reason about its existence. The uncertainty in energy of this transition is believed to be within 3 keV.

[f]The intensity flow from the isomeric $11/2^-$ level in band 9 is not included.

[g]Transitions not shown in the level scheme.
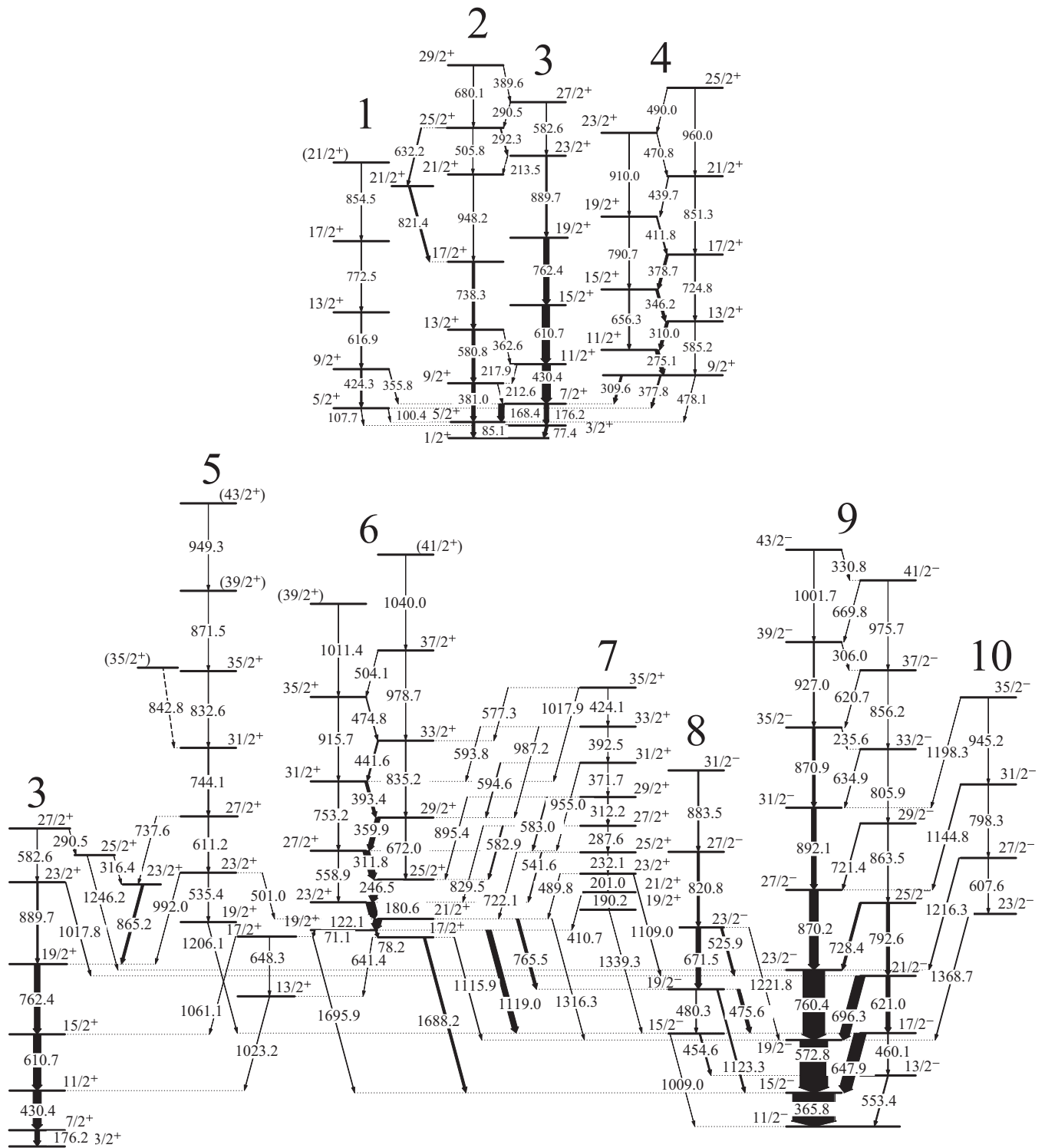
FIG. 1. The level scheme of ^{125}Cs deduced from the present paper. The transition energies are given in keV, and their relative intensities are indicated by the widths of the arrows. Uncertain spin and parity assignments are given in brackets.

shown in Fig. 2(b) does show the existence of two γ rays with nearly the same energy of 310 keV. Moreover, the coincidence intensity between them is obviously much greater than all of those coincidence intensities relevant to contamination lines seen in Figs. 2(a) and 2(b). In particular, the coincidence

relations shown in Figs. 2(a) and 2(b) for the 168-keV line and 310-keV doublet lines cannot be accommodated by any other nuclei contained in our data except ^{125}Cs. In contrast, the observed coincidences can be accommodated by ^{125}Cs self-consistently. Further arguments can be found from spectra

◆ : ^{117}In ;   ▲ : ^{123}I ;   ■ : ^{126}Cs ;   ▼ : ^{126}Xe ;   ● : ^{120}Sn ;   ▶ : ^{124}I
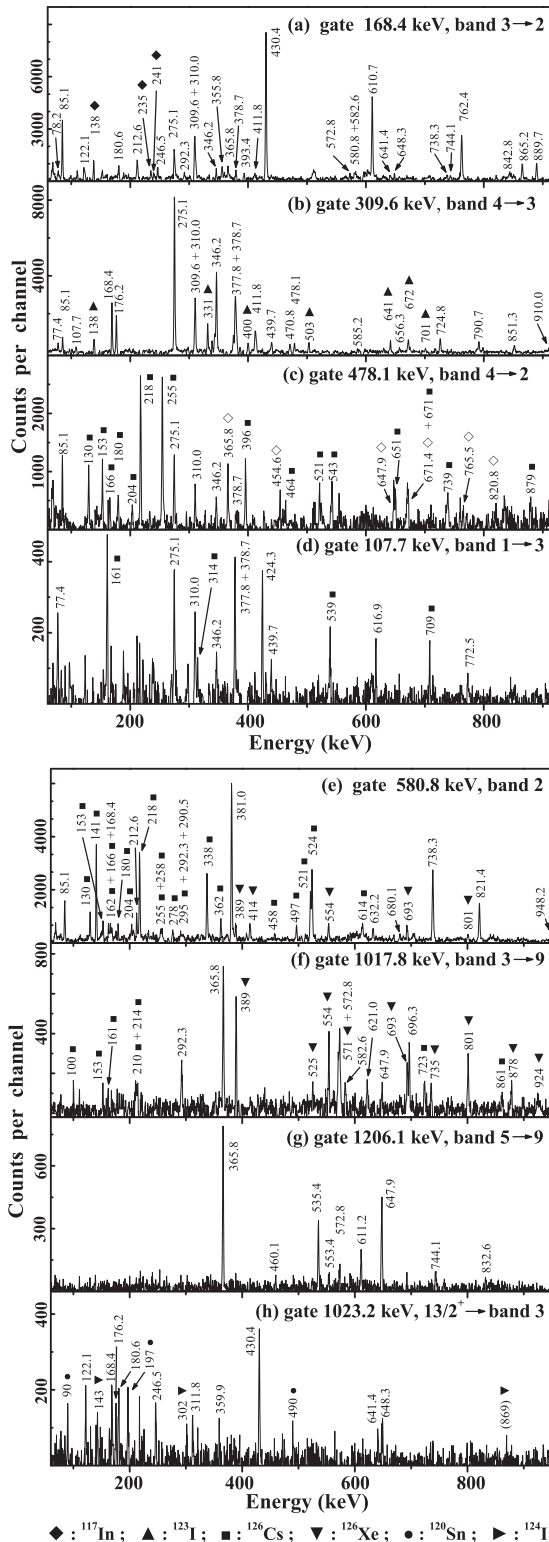
FIG. 2. Examples of coincidence spectra for ^{125}Cs. Transitions energies marked with solid symbols correspond to contaminations from the other nuclei as indicated at the bottom of the figure. The coincidence relationships shown for contamination nuclei can be verified from Refs. [36] (^{117}In), [3,37] (^{123}I), [6,33] (^{126}Cs), [35] (^{126}Xe), [38] (^{120}Sn), and [39] (^{124}I). The open rhombus symbols in (c) correspond to contaminations from bands 8 and 9 in ^{125}Cs. The contaminations from ^{126}Cs shown in (e) result from an unreported

gating on transitions which is in coincidence with only one component of the doublet, and Figs. 2(c) and 2(d) provide two examples of such spectra where the line at 310 keV shrinks remarkably as compared with other lines. Similarly, it can be verified that the line at 378 keV shown in Figs. 2(b) and 2(d) is also a doublet from ^{125}Cs. In fact, the doublet nature of the 378-keV line can also be inferred from Fig. 1 in Ref. [11] where the line at 378 keV shows a broad shape obviously inconsistent with the expectation for a single line and its coincidence intensity is anomalously greater than that of the 346-keV line.

Band 3 was previously observed up to $23/2^+$. In our paper, we confirm the band and extend it up to the $27/2^+$ level by a 582.6-keV transition. Different spin-parity assignments ($5/2^+$ and $3/2^+$) to the 77-keV state at the bottom of band 6 were performed in previous different studies [10–14]. In our paper, the ADO ratio deduced for the 176.2-keV transition feeding this 77-keV state is consistent with $E2$ multipolarity. In addition, the absence of a γ transition from the $9/2^+$ bandhead of band 4 to the 77-keV state also favors the $3/2^+$ rather than the $5/2^+$ assignment.

Bands 1 and 2 are two structures newly identified from this study. The nuclide assignment for them is based on the observations of a number of transitions connecting the two structures to known states in ^{125}Cs. Figures 2(d) and 2(e) display two examples of coincidence spectra for bands 1 and 2. The 185-keV excitation energy of the $5/2^+$ level in band 1 and the 100.4- and 107.7-keV transitions depopulating this level are all in nice agreement with preexisting results of a level observed from the decay of ^{125}Ba [9,10]. Therefore, the two levels disclosed from the present in-beam study and the previous decay study [9] must be the same one. Three candidate spin values, i.e., 1/2, 3/2, and 5/2, were suggested for the level at 185 keV in previous studies [9,10]. In the present paper, the 100.4- and 107.7-keV linking transitions are not intense enough for obtaining meaningful ADO ratios. Fortunately, however, the presence of an intense 377.8-keV γ transition decaying from the $9/2^+$ state of band 4 to the 185-keV state in band 1 excludes the possibilities of 1/2 and 3/2 spin assignments, specifying the $5/2^+$ assignment for the 185-keV level in band 1. This assignment is further supported by the ADO ratio measured for the 355.8-keV transition connecting band 1 to band 3. The spin and parity assignments for levels in band 2 are relatively straightforward because many linking transitions exist between bands 2 and 3. The linking pattern and the ADO ratios measured for some relatively clean intense transitions both favor the spin-parity assignments for band 2 as shown in Fig. 1.

A number of interlinking dipole transitions are observed between bands 2 and 3 at the low spin region, and such transitions attenuate and eventually vanish with increasing spin. However, at the upper part of bands 2 and 3, they emerge

cascade which consists of 614-, 581-, and 524-keV transitions and feeds the (12^+) level in band 2 of ^{126}Cs [6]. The contaminations from ^{126}Xe shown in (f) result from an unreported 1018.0-keV transition which feeds the 14^+ level in the ground band of ^{126}Xe [35].

again. Meanwhile, the energies of the $\Delta I = 2$ transitions decrease considerably, reflecting an onset of upbend or even backbend in the alignment plot versus rotational frequency. These features may suggest the emergence of a new $\Delta I = 1$ band involving the excitations of two quasineutrons or protons.

Band 5 was also established in the recent work by Singh *et al.* [14]. However, they failed to establish the decay of this band to lower known states and had to assume spin-parity assignments for the band on the basis of a comparison with a similar band in ^{123}Cs [21,28]. In our paper, the position of a previously reported [14] 843-keV transition in this band could not be confirmed, and meanwhile, the band has been extended down by the addition of a new 535.4-keV $E2$ transition. Moreover, the decays of this band to lower known states have been firmly established as shown in Fig. 1. Spin-parity assignments for levels in this band were performed mainly on our ADO data. Interestingly, the result agrees well with the assumption by Singh *et al.* [14].

Band 6, consisting of intense $\Delta I = 1$ interweaving transitions along with weaker $E2$ crossover transitions, was first identified by Hughes *et al.* [12]. It decays into band 9 through three intense transitions with energies of 765, 1117, and 1686 keV, among which the 765-keV transition was found to have a nonzero mixing ratio ($\delta = -0.25 \pm 0.15$) and was thereby assigned a multipolarity $M1$ rather than $E1$. Thus band 6 was assigned a negative parity by Hughes *et al.* [12]. However, this assignment had been revised in the recent study by Singh *et al.* [14]. The reason of their revision is essentially some model-dependent theoretical considerations in the configuration assignment for band 6. Singh *et al.* assigned band 6 a positive-parity $\pi h_{11/2} \otimes \nu h_{11/2} \otimes \nu h_{7/2}$ configuration [14] instead of the negative-parity $\pi g_{7/2} \otimes \nu h_{11/2} \otimes \pi g_{7/2}$ configuration proposed by Hughes *et al.* [12]. In this paper, we have endeavored to make parity assignment for band 6 utilizing our good quality data sets. As seen in Fig. 1, in addition to the newly established decay paths finally down to the positive-parity band 3, many γ transitions depopulating band 6 to band 9 have been established. However, no $\Delta I = 2 \gamma$ transition linking band 6 to band 9 could be found. In view of the fact that band 6 shows a strong tendency to decay down into band 9, it is expected that $E2$ linking transitions would occur with appreciable intensities if bands 6 and 9 had the same parity. Therefore, the failure in finding such a $\Delta I = 2$ candidate linking γ transition strongly supports the positive-parity assignment for band 6.

Band 7 comprises eight transitions, among which the top three transitions had also been reported in the previous study by Singh *et al.* [14] whereas the lower five transitions are newly observed from this paper. As seen from Fig. 1, band 7 feeds strongly into band 6, and the linking pattern alone can imply that band 7 is a dipole band having the same parity with band 6. Further considerations including ADO data also support this conclusion.

Only two $E2$ transitions have been observed in band 8 prior to this paper. An 883.5-keV and a 480.3-keV transition have now been added on its top and at its bottom, extending the band up to $31/2^-$ and down to $15/2^-$, respectively. In comparison to band 10, band 8 seems to be a better candidate for the γ band based on the coupling of the $h_{11/2}$ proton to the γ vibration

of the core. It is noticed that, in odd-A Cs isotopes, ^{125}Cs is the second case after ^{131}Cs [19,20] where the $15/2^-$ level in the γ band is observed. A $13/2^-$ level in the $\alpha = +1/2$ unfavored signature of band 9 was tentatively suggested by Hughes *et al.* [12] but was removed from the level scheme by Singh *et al.* [14]. In this paper, the existence of that $13/2^-$ level is confirmed by the observed coincidences associated with the 460.1- and 553.4-keV transitions. Moreover, their order has also been firmly determined by the 454.6-keV transition depopulating the $15/2^-$ level in band 8. The contaminated coincidence spectrum shown in Fig. 2(c) lends support for the existence of the $13/2^-$ level in band 9.

IV. DISCUSSIONS

For the $_{55}$Cs nuclei, the active orbitals near the proton Fermi surface are $g_{7/2}[422]3/2^+, d_{5/2}[420]1/2^+$, the $g_{9/2}[404]9/2^+$ extruder, and the unique-parity $h_{11/2}[550]1/2^-$ intruder. Low-lying states in odd-A Cs nuclei are expected to be intimately related to these orbitals. In ^{125}Cs, the low-lying bands 4 and 9 show very distinct structures, and they had been previously assigned to the $g_{9/2}[404]9/2^+$ and $h_{11/2}[550]1/2^-$ configurations, respectively [12,14]. Since the $g_{7/2}[422]3/2^+$ orbital is the only positive-parity orbital expected to have the $\alpha = -1/2$ signature favored, band 3 with $\alpha = -1/2$ must be built upon the $g_{7/2}[422]3/2^+$ orbital, although there may be some mixing from its pseudospin partner $d_{5/2}[420]1/2^+$ orbital. The remaining bands 1 and 2, both having $\alpha = +1/2$, must relate to the unfavored signature of the $g_{7/2}[422]3/2^+$ configuration and the favored signature of the $d_{5/2}[420]1/2^+$ configuration. In order to find out the respective counterpart configurations of bands 1 and 2, it is instructive to make a survey of similar structures in adjacent odd-A Cs isotopes. Figure 3 presents a comparison of such structures in ^{125,127,129}Cs. A striking
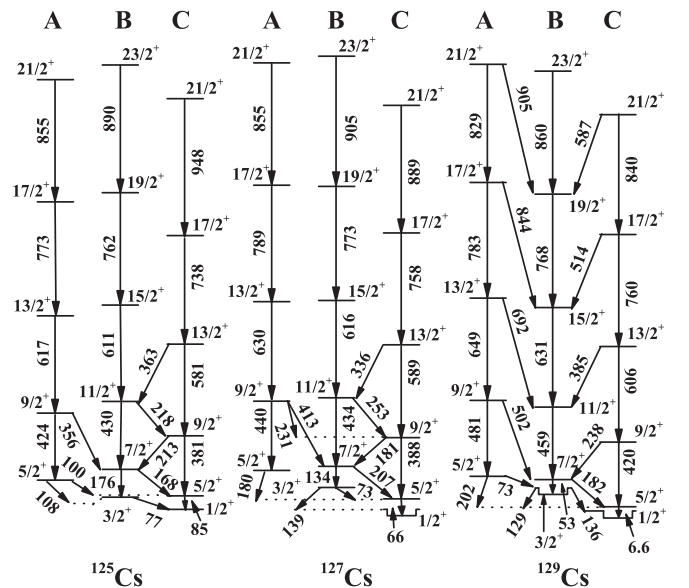
FIG. 3. Comparison of the observed low-spin structures associated with the $\pi g_{7/2}$ and $\pi d_{5/2}$ configurations in ^{125,127,129}Cs. Data are taken from Ref. [15] for ^{127}Cs and from Refs. [17,18,40] for ^{129}Cs.

feature can be found from Fig. 3: Bands B and C feed into each other at low spins via a number of linking transitions whereas only a few transitions exist between bands B and A. This feature tempts one to interpret bands B and C as a pair of signature partners in a common configuration. Indeed, in the earlier studies on ^{127}Cs [15] and ^{129}Cs [16], bands B and C, respectively, were interpreted as the favored and unfavored signature of the $\pi g_{7/2}[422]3/2^+$ configuration whereas band A was interpreted as the favored signature of the $\pi d_{5/2}[420]1/2^+$ configuration. Similar considerations were also applied to the neighboring $Z = 53$ iodine isotopes [3]. However, in the recent study by Sihotra *et al.* [18], bands B and C in ^{129}Cs were observed to be populated with nearly equal intensity, which was thought to be unreasonable by the authors if bands B and C are the favored and unfavored signature partners in the earlier assigned $\pi g_{7/2}$ configuration. Instead, Sihotra *et al.* [18] proposed an alternative prescription, interpreting band C in ^{129}Cs as the favored signature of the $\pi d_{5/2}[420]1/2^+$ configuration and bands A and B as the unfavored and favored signatures of the $\pi g_{7/2}[422]3/2^+$ configuration, respectively.

The $\pi g_{7/2}[422]3/2^+$ and $\pi d_{5/2}[420]1/2^+$ Nilsson orbitals are close-lying pseudospin partners, and a strong admixture of their wave functions is expected. Therefore, the observation of relatively stronger admixture between bands B and C does not necessarily mean that they are a signature pair. On the other hand, we also do not think it is safe to distinguish between unfavored and favored signatures according to their observed population intensities. In fact, the population of a band in fusion-evaporation reactions may depend on several conditions in addition to the favored or unfavored character. For instance, it is possible that an unfavored signature is populated with larger intensity than its favored signature partner provided that the unfavored band undergoes a band crossing at a lower rotational frequency and with a larger alignment gain. In particular, in the present case of ^{125}Cs, band C is observed to be populated with remarkably lower intensity than band B, compatible with the earlier prescription proposed for ^{127}Cs [15] and ^{129}Cs [16]. Anyway, it seems not so straightforward to judge which one is the signature partner of band B between bands A and C shown in Fig. 3. In aid to judging between the two possibilities, a plot showing the energy staggering behaviors is displayed in Fig. 4 where the upper row is made under the assumption (abbreviated as AI in the following) that bands B and A are a signature pair and the lower row under the another assumption (abbreviated as AII). Striking similarities can be seen among the three Cs isotopes under every assumption, corroborating the conclusion that the band labeled with the same letter in Fig. 3 is from the same configuration. Another remarkable feature in Fig. 4 is the low-spin signature inversion under AII. The phenomenon of signature inversion has been extensively reported in doubly nuclei at low spins [1] and in odd-*A* nuclei at high spins [41]. However, no firm evidence of systematic signature inversion has been reported in the literature for odd-*A* systems at low spins. Low-spin signature inversion in odd-*A* nuclei is either not expected according to the standard cranked-shell-model (CSM) unless a considerably large positive triaxiality is introduced [42]. Total-Routhian-Surface calculations taking ^{127}Cs [15] and ^{123}Cs [21] as examples indicate that the low-lying
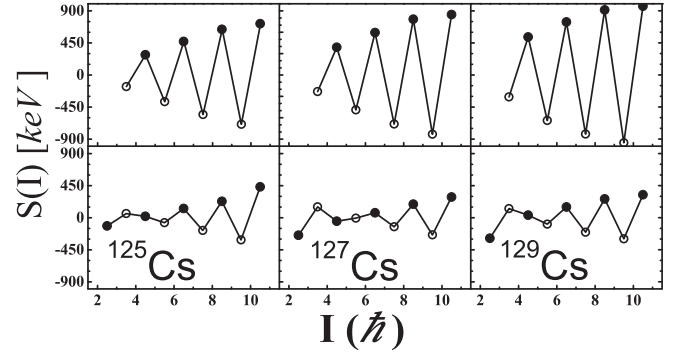
FIG. 4. Plot illustrating the energy staggering behavior as a function of spin for the bands shown in Fig. 3. $S(I)$ is defined as $[E(I) - E(I-1)] - [E(I+1) - E(I) + E(I-1) - E(I-2)]/2$. See the text for further details.

positive-parity bands in odd-*A* Cs isotopes of this region have normal prolate deformation with $\gamma \approx 0°$ below band crossing, inconsistent with the picture of large positive triaxiality. Therefore, it is hard to understand the occurrence of the low-spin signature inversion shown in Fig. 4 under AII. In contrast, the signature-splitting behavior under AI is in good agreement with the expectation from CSM [42]. As seen in Fig. 4, under AI, the amplitude of signature splitting increases with increasing spin, in accordance with the increase in Coriolis effect with increasing rotational frequency. Therefore, AI is believed by us to be more reasonable than AII.

The above proposal is further supported qualitatively by CSM calculations. In Fig. 5, we present a quasiproton diagram calculated using the standard CSM [42]. It can be seen from Fig. 5 that, without introducing a large positive triaxiality, a crossing between the $\pi g_{7/2}[422]3/2^+(a = -1/2)$ and $\pi d_{5/2}[420]1/2^+(a = +1/2)$ orbitals may occur at a low
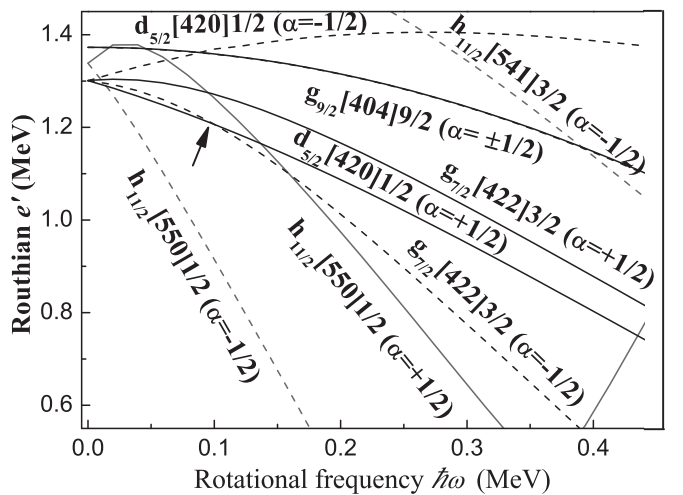
FIG. 5. Quasiproton Routhians for cesium isotopes as a function of rotational frequency calculated at $\varepsilon_2 = 0.25, \varepsilon_4 = 0, \gamma = 0°$, and $\Delta_p = 1.3$ MeV. The levels are marked with their Nilsson configurations. An arrow is inserted to indicate the crossing between the two configurations under discussions.

rotational frequency. Such a crossing provides a qualitative explanation for the so-called signature inversion between bands B and C as implied in Fig. 4. The $\pi g_{7/2}[422]3/2^+(a = -1/2)$ band has a higher bandhead excitation energy but carries larger alignment (manifested as the negative slope of the orbitals shown in Fig. 5) than the $\pi d_{5/2}[420]1/2^+(a = +1/2)$ band, resulting in a crossing between them with increasing spin.

Other evidence supporting AI is the decay pattern at low spins as shown in Fig. 3. So far, no observation of a transition connecting the $5/2^+$ level of band A to the ground state with $I^\pi = 1/2^+$ has been reported in three nuclei. In the current study on the case of ^{125}Cs, special attempts have been made to look for such a transition, however, no evidence can be found. In sharp contrast, transitions from the $5/2^+$ level in band C to the $1/2^+$ ground state have been reported in all of three nuclei, irrespective of how close the two levels lie. In particular, the corresponding transition in ^{125}Cs is observed to be quite intense. As seen in Figs. 2(a)–2(c), the peak corresponding to the 85.1-keV $5/2^+ \rightarrow 1/2^+$ transition stands out, despite the significant internal conversion associated with low-energy transitions. The above striking difference between the two $5/2^+$ levels of bands A and C strongly suggests that the $I^\pi = 1/2^+$ ground state in three nuclei is a member state of band C rather than that of band A. Since a rotational band built on the low-j $d_{5/2}[420]1/2^+$ configuration may start with $I = K = 1/2$, AII would result in an abnormal absence of the $I = 1/2$ level in the $d_{5/2}[420]1/2^+$ band.

Earlier studies (e.g., Ref. [43] and references therein) interpreted the lowest $1/2^+$ state in odd-A Cs isotopes as resulting from the coupling of some vibrational degrees of freedom to the $d_{5/2}$ or $g_{7/2}$ orbitals. In view of the observation that an intense $E2$ transition occurs systematically between the $5/2^+$ and the $1/2^+$ levels in bands C of ^{125,127,129}Cs, we interpret the $I^\pi = 1/2^+$ ground state in these nuclei as the bandhead of the $d_{5/2}[420]1/2^+$ band. Likewise, the $3/2^+$ level of band B in these nuclei is interpreted as the bandhead of $\pi g_{7/2}[422]3/2^+$ band. The same interpretations were also proposed [22] for the lowest $1/2^+$ and $3/2^+$ states in the neighboring ^{123}Cs according to predictions from the IBFM-2 and CQPC models. In comparison with structures above the $I = j$ state, the energy spaces below the $I = j$ state in bands $B(j = 7/2)$ and $C(j = 5/2)$ are highly compressed. This irregularity casts doubt on the present interpretation about the $1/2^+$ and $3/2^+$ states in ^{125,127,129}Cs. In fact, however, similar feature is often seen in rotational bands with high-j and medium- to low-Ω in odd-A nuclei. For example, in the $h_{11/2}$ band of the nearby nucleus ^{123}Xe [44], the $11/2^- \rightarrow 7/2^-$ transition energy is only 57 keV, significantly compressed in comparison with the 456 and 617 keV of the $15/2^- \rightarrow 11/2^-$ and $19/2^- \rightarrow 15/2^-$ transitions. As discussed in great detail

by Kreiner *et al.* [45], this kind of compression is intimately related to the perturbation from Coriolis effects [46] in rotating nuclei. Coriolis effects are expected [46] to become larger with decreasing moment of inertia. The deformation and the moment of inertia drop for heavier Cs isotopes. Hence, one expects an increase in the Coriolis effects with increasing mass number in odd-A Cs isotopes. What is seen in Fig. 3 is indeed consistent with this picture. Moreover, when going from ^{129}Cs into ^{131}Cs [19,20], both the positions of the $3/2^+$ and $7/2^+$ levels in band B and the positions of the $1/2^+$ and $5/2^+$ levels in band C are inverted, reflecting drastic enhancement of the Coriolis effects. At the same time, the distance between various active Nilsson orbitals and the Fermi surface varies with deformation, leading to the interesting and complex variations of bandhead energies with the mass number along the cesium isotopic chain as shown in Fig. 6 in Ref. [22]. To reproduce the bandhead energies along the long chain of Cs isotopes is of significance for theoretical studies.

V. SUMMARY

To summarize, the excited states in ^{125}Cs were populated via the ^{116}Cd $(^{14}$N$, 5n)$ reaction using the Nordball-multidetector system at the Niels Bohr Institute in Denmark. The bandhead excitation energies of the $h_{11/2}$ and $g_{9/2}$ bands determined in previous studies are revised on the basis of direct and firm experimental evidence, making a delicate systematic study of bandhead energies in odd-A isotopes possible. More than 50 new γ rays are added into the level scheme. Relative intensities and ADO ratios of γ rays in ^{125}Cs are obtained. Two new bands are identified for the first time. Their configurations at low spins are assigned mainly based on observed spectroscopic features; one of the new bands is assigned the favored signature of the $\pi d_{5/2}[420]1/2^+$ configuration, and another is assigned the unfavored signature of the $\pi g_{7/2}[422]3/2^+$ configuration. This set of configuration assignments agrees with the prescription proposed for ^{129}Cs by Sihotra *et al.* [18] and calls for a reappraisal of the configuration assignments for similar bands in ^{127}Cs and even in odd-A iodine isotopes. The observed lowest $1/2^+$ and $3/2^+$ states in ^{125}Cs are proposed to be the bandheads of the $d_{5/2}[420]1/2^+$ and $g_{7/2}[422]3/2^+$ configurations, respectively. It is demonstrated that a plain and consistent understanding about the energy spectra of the $\pi g_{7/2}$ and $\pi d_{5/2}$ levels in odd-A Cs isotopes is accessible in the framework of cranked shell model.

[1] Y. Liu, J. Lu, Y. Ma, S.i Zhou, and H. Zheng, Phys. Rev. C **54**, 719 (1996).

[2] R. A. Wyss, A. Johnson, J. Nyberg, R. Bengtsson, and W. Nazarewicz, Z. Phys. A: At. Nucl. **329**, 255 (1988).

[3] S.-Y. Wang *et al.*, J. Phys. G **32**, 283 (2006).

[4] I. Schneider *et al.*, Phys. Rev. C **60**, 014312 (1999).

[5] R. Wadsworth *et al.*, Phys. Rev. C **62**, 034315 (2000).

[6] S. Wang, Y. Liu, T. Komatsubara, Y. Ma, and Y. Zhang, Phys. Rev. C **74**, 017302 (2006).

[7] K. Selvakumar *et al.*, Phys. Rev. C **92**, 064307 (2015).

[8] O. B. Dabbousi, M. H. Prior, and H. A. Shugart, Phys. Rev. C **3**, 1326 (1971).

[9] R. Arlt, A. Jasinski, W. Neubert, and H.-G. Ortlepp, Acta Phys. Pol., B **6**, 433 (1975).

[10] J. Katakura, Nucl. Data Sheets **112**, 495 (2011).

[11] U. Garg, T. P. Sjoreen, and D. B. Fossan, Phys. Rev. C **19**, 217 (1979).

[12] J. R. Hughes, D. B. Fossan, D. R. LaFosse, Y. Liang, P. Vaska, and M. P. Waring, Phys. Rev. C **44**, 2390 (1991).

[13] M. Sugawara, H. Kusakari, T. Murakami, and T. Kohno, Eur. Phys. J. A **2**, 237 (1998).

[14] K. Singh *et al.*, Eur. Phys. J. A **27**, 321 (2006).

[15] Y. Liang, R. Ma, E. S. Paul, N. Xu, D. B. Fossan, and R. A. Wyss, Phys. Rev. C **42**, 890 (1990).

[16] L. Hildingsson, W. Klamra, T. Lindblad, F. Lidén, Y. Liang, R. Ma, E. S. Paul, N. Xu, D. B. Fossan, and J. Gascon, Z. Phys. A: Hadrons Nucl. **340**, 29 (1991).

[17] Zhao Yan-Xin *et al.*, Chin. Phys. Lett. **26**, 092301 (2009).

[18] S. Sihotra *et al.*, Phys. Rev. C **79**, 044317 (2009).

[19] S. Sihotra *et al.*, Phys. Rev. C **78**, 034313 (2008).

[20] R. Kumar, K. Singh, D. Mehta, N. Singh, S. S. Malik, E. S. Paul, A. Görgen, S. Chmel, R. P. Singh, and S. Muralithar, Eur. Phys. J. A **24**, 13 (2005).

[21] Kuljeet Singh *et al.*, Eur. Phys. J. A **25**, 345 (2005).

[22] A. Gizon *et al.*, Eur. Phys. J. A **8**, 41 (2000).

[23] J. R. Hughes, D. B. Fossan, D. R. LaFosse, Y. Liang, P. Vaska, M. P. Waring, and J.-Y. Zhang, Phys. Rev. C **45**, 2177 (1992).

[24] C.-B. Moon, T. Komatsubara, and K. Furuno, J. Korean Phys. Soc. **38**, 83 (2001).

[25] F. Liden *et al.*, Nucl. Phys. A **550**, 365 (1992).

[26] X. Sun *et al.*, Phys. Rev. C **51**, 2803 (1995).

[27] J. F. Smith *et al.*, Phys. Rev. C **63**, 024319 (2001).

[28] A. K. Singh *et al.*, Phys. Rev. C **70**, 034315 (2004).

[29] T. Komatsubara *et al.*, Nucl. Phys. A **557**, 419c (1993).

[30] Bent Herskind, Nucl. Phys. A **447**, 395 (1986).

[31] S. Törmänen *et al.*, Nucl. Phys. A **613**, 282 (1997).

[32] M. Piiparinen *et al.*, Nucl. Phys. A **605**, 191 (1996).

[33] S. Wang, Y. Liu, Y. Ma, T. Komatsubara, and Y. Zhang, Phys. Rev. C **75**, 037302 (2007).

[34] Y.-X. Zhao, T. Komatsubara, Y.-J. Ma, Y.-H. Zhang, S.-Y. Wang, Y.-Z. Liu, and K. Furuno, Chin. Phys. Lett. **26**, 082301 (2009).

[35] C. Rønn Hansen *et al.*, Phys. Rev. C **76**, 034311 (2007).

[36] R. Lucas *et al.*, Eur. Phys. J. A **15**, 315 (2002).

[37] R. Goswami, B. Sethi, and P. Banerjee, and R. K. Chattopadhyay, Phys. Rev. C **47**, 1013 (1993).

[38] A. Astier *et al.*, Phys. Rev. C **85**, 054316 (2012).

[39] C. B. Moon, G. D. Dracoulis, R. A. Bark, A. P. Byrne, P. M. Davidson, A. N. Wilson, T. Kibedi, G. J. Lane, and A. M. Baxter, Department of Nuclear Physics 2002 Australian National University, Annual Report, 2003, p.15.

[40] J. Timar, Z. Elekes, and B. Singh, Nucl. Data Sheets **121**, 143 (2014).

[41] C.-H. Yu *et al.*, Nucl. Phys. A **489**, 477 (1988).

[42] R. Bengtsson and S. Frauendorf, Nucl. Phys. A **327**, 139 (1979).

[43] I. V. Goldstein, and A. G. de Pinho, Phys. Rev. C **4**, 653 (1971).

[44] A. Gade, H. Meise, I. Wiedenhöver, A. Schmidt, and A. Gelberg, Nucl. Phys. A **686**, 3 (2001).

[45] A. J. Kreiner, l. Davidson, M. Davidson, D. Abriola, C. Pomar, and P. Thieberger, Phys. Rev. C **36**, 2309 (1987).

[46] F. S. Stephens, Rev. Mod. Phys. **47**, 43 (1975).